МИНЕРАЛОГИЧЕСКАЯ КРИСТАЛЛОГРАФИЯ

GRAIN BOUNDARIES IN MINERALS: ATOMIC STRUCTURE, PHASE TRANSITIONS, AND EFFECT ON STRENGTH OF POLYCRYSTALS

© 2021 г.   A. B. Mazitov[1, 2], * and A. R. Oganov[3], **

[1]*Moscow Institute of Physics and Technology, Institutsky lane, 9,, Dolgoprudny, 141700 Russia*
[2]*Dukhov Research Institute of Automatics (VNIIA), Suschevskaya str., 22,, Moscow, 127055 Russia*
[3]*Skolkovo Institute of Science and Technology, Skolkovo Innovation Center,*
Nobel str., 3 , Moscow, 121205 Russia
*e-mail: arslan.mazitov@phystech.edu
**e-mail: a.r.oganov@mail.ru

Grain boundaries (GBs) and interfaces in polycrystalline materials are significant research subjects in the field of materials science. Despite a more than 50-year history of their study, there are still many open questions. The main challenge in studying interfacial structures is the extreme complexity of their experimental and theoretical observation and description. The presence of phase-like states at grain boundaries called *complexions* requires even more effort in their study. Here, we demonstrate the effect of grain boundaries on the properties of polycrystalline minerals on the example of the $\Sigma5(310)[001]$ grain boundary in periclase (MgO). Using the combination of extended evolutionary algorithm USPEX and modern machine-learning interatomic potentials, we explore the configuration space of the specified grain boundary and predict its possible phase-like states. In addition to the widely studied CSL-type structure, we found several stable GB complexions with various atomic densities at the boundary plane. Analysis of grain boundary excess volume of the structures revealed the successive stages of GB failure under the tensile stress applied in the normal direction of the boundary plane. Our results demonstrate that interfacial chemistry and structural diversity can be surprisingly rich even in seemingly simple and thoroughly investigated materials. The phenomena we observe here are not unique to MgO and should be general.

Keywords: crystal structure prediction, grain boundaries, grain boundary complexions, machine learning, interatomic potentials, density functional theory

DOI: 10.31857/S086960552105004X

INTRODUCTION

Grain boundaries and interfaces are known to strongly influence the mechanical and transport behavior of polycrystalline materials (Sutton, Balluffi, 1995). Many efforts have been made in the last decades (Panchal et al., 2013) to establish the relation between local interfacial structure and chemistry and various phenomena such as microstructure evolution (Mott, 1948; Beck, Sperry, 1950; Burke,Turnbull, 1952), segregation (Lejček et al., 2017), creep (Langdon, 1970; Raj, Ashby, 1971; Watanabe, 1982; Chen, Schuh, 2007), fatigue (Tanaka et al., 1986; Sangid et al., 2011; Sangid, 2013; Musinski, McDowell, 2016), fracture (Watanabe, Tsurekawa, 1999, 2004) and corrosion (Lin et al., 1995; Lehockey et al., 1997; Shimada et al., 2002). The intrinsic complexity of both homo- and heterophase interfaces requires at least five parameters to uniquely describe their misorientation angle and boundary plane orientation (Sutton, Balluffi, 1995). Thus, various approaches including Coincidence Site Lattice (CSL) and Displacement Shift Complete (DSC) lattice (Sutton, Balluffi, 1995), dichromatic patterns

and complexes (based on Shubnikov groups) (Shubnikov, Koptsik, 1972; Pond, Bollmann, 1979; Pond, Vlachavas, 1983), and Bollman's 0-lattice theory (Bollmann, 1967; Smith, Pond, 1976) were introduced to provide this description. Recent experimental studies show that the chemical and structural diversity of grain boundaries (GBs) can be even greater. According to Dillon et al. (Dillon et al., 2007; Dillon, Harmer, 2007), and Cantwell et al. (Cantwell et al., 2014, 2016), GBs can demonstrate phase-like behavior similarly to bulk crystals and undergo first-order transitions called *complexion* transitions at the same macroscopic crystallographic parameters. This makes the study of grain boundary structure and its relation to the properties of materials even more difficult.

Experimental observation of grain boundaries and complexion transitions at the atomic scale is extremely complicated since it requires a thorough sample growth and preparation followed by accurate *in situ* high-resolution microscopy analysis in ultrahigh vacuum (Chen et al., 2008; Cantwell et al., 2020). On the other hand, theoretical simulations of GBs are relatively cheap since they are often carried out within classical molecular dynamics with empirical interatomic potentials, where CSL theory is used for creating the initial orientation of crystallites (Béré et al., 2002; Uberuaga, Bai, 2011; Uberuaga et al., 2013; Frolov et al., 2013, 2015; Fujii et al., 2019). However, this approach cannot provide a general description of all GB phases and complexion transitions for given GB crystallographic parameters, being limited only to manually prepared structural patterns. Furthermore, such calculations can suffer from inaccuracy of both CSL approximation and errors of empirical interatomic potentials. Despite the non-trivial nature of the problem, an effective method of grain boundary structure prediction based on evolutionary algorithm USPEX (Oganov, Glass, 2006; Oganov et al., 2011; Lyakhov et al., 2013), was recently proposed and successfully applied to the study of GB phase behavior in elemental metals (Frolov, Setyawan et al., 2018; Frolov, Zhu et al., 2018; Zhu et al., 2018; Meiners et al., 2020).

EVOLUTIONARY ALGORITHM

Here, we extend this method to grain boundaries in compounds, and boost its efficiency and reliability by using accurate machine learning interatomic potentials. USPEX was previously used to study bulk crystals at zero and finite temperatures (Kruglov et al., 2021), free surfaces (Zhu et al., 2013), two-dimensional materials (Zhou et al., 2016), epitaxial thin films (Mazitov, Oganov, 2021), nanoclusters (Lepeshkin et al., 2018), and grain boundaries in single-component systems (Zhu et al., 2018). The interface system in our method is represented by a thick slab immersed in vacuum and consisting of three parts: two bulk regions and an interfacial region located between them (Fig. 1).

Our algorithm optimizes the structure of the interface keeping bulk regions unchanged. The first generation of individuals is produced with a topological random structure generator (Bushlanov et al., 2019), while all subsequent generations are created by variation operators using the best representatives of the previous generation as parents. There are four variation operators implemented in our method: (1) heredity, (2) softmutation, (3) transmutation, and (4) addition/deletion. The first one creates offspring from two randomly sliced parents by combining their fragments. The remaining operators act on the structure of a single parent by shifting the atoms along with the softest vibrational modes (2), changing the chemical identity of some atoms (3), and adding (or deleting) the atoms according to their coordination number (4). A certain percentage of random structures are included in each generation to ensure diversity of the population. All structures are relaxed and ranked by fitness function based on their energy. This process is repeated iteratively until the set of the fittest individuals remains unchanged for a sufficiently large number of generations.

MACHINE LEARNING INTERATOMIC POTENTIALS

The evolutionary search typically requires hundreds or even thousands of structure relaxations, which should be performed with high accuracy to properly determine the ground state of the system. In contrast to crystal structures, the atomic structures of computationally studied grain boundaries are usually larger by an order of magnitude, which makes their prediction
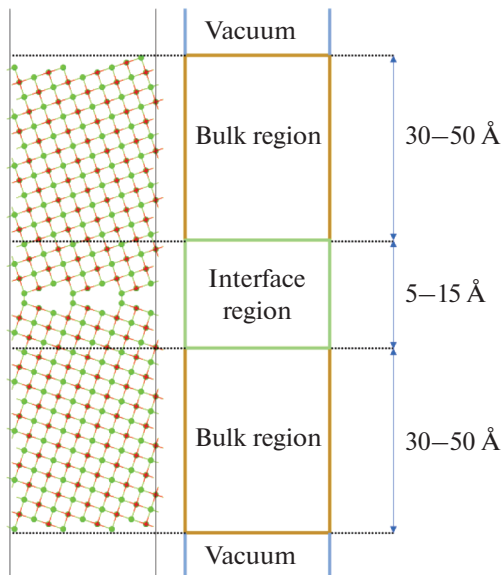
Fig. 1. Representation of interfaces in our evolutionary algorithm. Structure optimization is performed in the interface region, while the bulk regions are frozen. Both bulk regions end up with free surfaces followed by vacuum layers that exclude the periodic replica interactions. Thickness of the interface region is 5 to 15 Å, while the bulk regions are usually 30 to 50 Å thick.

Рис. 1. Модель межзеренной границы в нашем эволюционном алгоритме. Оптимизация структуры происходит в приграничной области, в то время как области кристаллитов остаются фиксированными в ходе расчета. Обе области кристаллитов оканчиваются свободными поверхностями, за которыми следует слой вакуума, исключающий взаимодействие периодических копий межзеренной границы друг с другом. Толщина приграничной области находится в диапазоне от 5 до 15 Å, в то время как области кристаллитов обычно имеют толщину от 30 до 50 Å.

with the usage of *ab initio* relaxation practically unfeasible. Previous studies of grain boundaries in simple metals (Frolov et al., 2015, 2016; Frolov, Zhu et al., 2018; Meiners et al., 2020; Zhu et al., 2018) show that classical interatomic potentials in principle can be utilized for their simulation and structure prediction. However, the accuracy of these potentials is not always sufficient to reliably determine the ground state, both for bulk crystals and for grain boundaries. In this work, we replace classical potentials with an accurate machine learning (ML) interatomic potential using the MTP package (Shapeev, 2016), and utilize the two-stage relaxation scheme with two separately trained potentials. The first potential was actively trained on relaxation trajectories of random crystal structures generated by USPEX. It is designed to operate in a wide region of the phase space and perform the initial crude relaxation. The second potential was trained on molecular dynamics trajectories of bulk supercells with the addition of point defects and random deformations of the unit cell. Since there were no structures with free surfaces and grain boundaries in such a training set, we extended it with GB structures randomly generated with USPEX and preliminarily relaxed with the first potential. The resulting training set represents a relatively narrow region of the phase space, while the corresponding interatomic potentials turn out to be more accurate and can be used for a final structure relaxation. Data on energies, interatomic forces and stresses of the structures were obtained with density functional theory (DFT) with the generalized gradient approximation (Perdew et al., 1996) and projector-augmented wave method (Bloechl, 1994; Kresse, Joubert, 1999), as implemented in VASP code (Kresse, Furthmuller, 1996). Accuracy of the second interatomic po-

Table 1. Comparison of equilibrium lattice constant a_0 and elastic constants of MgO calculated with DFT and MTP.
Таблица 1. Сравнение равновесной постоянной решетки и упругих постоянных MgO, вычисленных с помощью DFT и MTP.

	a_0, Å	C_{11}, GPa	C_{12}, GPa	C_{44}, GPa
MTP	4.252	285	101	154
DFT	4.249	272	90	143

tential in prediction of equilibrium lattice constant a_0 and elastic constants C_{11}, C_{12}, and C_{44} is given in Table 1. For more information on ML interatomic potentials, the reader is referred to work (Podryabinkin, Shapeev, 2017).

RESULTS

We applied our method to study the atomic structure of $\Sigma5(310)[001]$ grain boundaries in mineral periclase (MgO). This boundary is a symmetric tilt boundary resulting from the simultaneous rotation of two (310) surface slabs by an angle of 36.9° around the [001] axis. Our choice of this particular GB orientation was conditioned by a presence of a sufficient number of studies in the literature suitable for comparison of the results. Being probably the most studied metal oxide, MgO is commonly utilized as a model system for more complex oxides. Grain boundaries are known to significantly affect various properties of polycrystalline metal oxides in a wide range of practically important applications, such as MOSFETs (Kukli et al., 2002; Yanev et al., 2008), fuel cells (Maier, 2000; Suzuki et al., 2001), gas sensors (Kosacki et al., 2005; Dey, 2018), varistors (Clarke, 1999), SQUIDs and high-Tc superconductors (Hilgenkamp, Mannhart, 2002). According to a large number of experimental and theoretical studies (Duffy, 1986; Yan et al., 1998b; Yan et al., 1998a; Parker, Harris, 1999; Harris et al., 2001; Harding, 2003; Wynblatt et al., 2003), point defects in MgO tend to segregate at grain boundaries and diffuse along them, which makes the properties of polycrystalline MgO depend considerably on GB structure. The evolutionary search was carried out for up to 100 generations with 30 individuals in each generation. The initial population of 30 GB structures with 4−16 MgO units (up to 32 atoms in the interface region) was produced by a topological random generator. The structures in subsequent generations were produced by heredity (40%) and softmutation (20%) operators, while the remaining 30% were produced randomly to diversify the population. The thickness of the grain boundary region was automatically adjusted according to the number of MgO units in the structure and the average atomic density of bulk MgO, while both bulk blocks were 50 Å thick. We also considered reconstructions of the grain boundary unit cell with a cell area up to 4 times larger than the original interface unit cell area. Structure relaxations and energy calculations were performed in two stages with the two ML potentials described above, using the LAMMPS package (Plimpton, 1995). Each relaxation stage consisted of a short finite-temperature molecular dynamics run followed by conjugate gradients minimization, where only the atoms of the GB region were allowed to move. Finally, for each GB structure, we calculated the value of the interface energy according to the formula

$$\gamma = \frac{1}{A}\left(E - 2E_s - N_{\mathrm{MgO}}\mu_{\mathrm{MgO}}\right),$$

where E is the energy of whole atomic block with grain boundary, two bulk regions and two free (310) surfaces, E_s is the (310) surface energy, N_{MgO}, μ_{MgO} are the number of MgO units in the structure and chemical potential of MgO, and is the area of the grain boundary.

Results of the evolutionary search are illustrated in Fig. 2. We represented each structure as a point on the phase diagram in (n, γ) space, where n is the atomic density on the grain boundary plane. To derive n, we first calculate the number of atoms in the system N and the

number of atoms in one (310) plane of the MgO bulk region $N_{\text{plane}}^{\text{bulk}}$. Finally, we calculate n as the ratio $\left(N \bmod N_{\text{plane}}^{\text{bulk}}\right)\!\Big/ N_{\text{plane}}^{\text{bulk}}$. Physical meaning of this quantity is the fraction of atoms from the ideal (310) plane located in the grain boundary plane. This approach, recently proposed by Zhu et al. (Zhu et al., 2018), separates structures with different atomic densities, considering them as grain boundary complexions. Our algorithm successfully found a widely known CSL-type structure (ID 587) with $n = 0$, which was extensively studied in previous works (Fujii et al., 2019; Harris et al., 2001; Uberuaga, Bai, 2011; Yan et al., 1998b) to be the most stable. Predicted value of its interface energy is $\gamma = 87 \,\text{meV}\big/\text{Å}^2$. Moreover, in addition to grain boundaries with standard atomic density ($n = 0$), various GB complexions with different atomic densities (ID 1570, ID 434, ID 252) were found. All these structures are essentially modifications of the ground state, which can be observed during grain boundary segregation and diffusion or complexion transitions. Interface energies of these structures, $\gamma = 102 \,\text{meV}\big/\text{Å}^2$ (ID 1570), $\gamma = 105 \,\text{meV}\big/\text{Å}^2$ (ID 434), and $\gamma = 102 \,\text{meV}\big/\text{Å}^2$ (ID 252), are also fairly close to the ground state.

The accuracy of MTP interatomic potential in prediction of the interface energy was subsequently tested on a subset of the best GB structures from the evolutionary search. We selected 25 structures for each value of n with various predicted γ including both stable and unstable structures, and calculated their interface energies with VASP, at DFT level of theory. Results of this accuracy test are presented in Fig. 3. MTP demonstrates an outstanding performance in prediction of the interface energy with a root-mean-squared error (RMSE) of $8.4 \,\text{meV}\big/\text{Å}^2$ or 6.7% with respect to mean value of γ in this set of structures. Moreover, the predicted interface energy of the ground state (ID 587) differs from DFT value only by $4.8 \,\text{meV}\big/\text{Å}^2$ while the atomic configuration of the DFT ground state is almost indistinguishable from that predicted by MTP.

Interface energies in $\Sigma 5 (310)[001]$ GBs are rather ordinary for ionic crystals. In Table 2, we compare our results with typical values of grain boundary formation energies in different substances: copper, tungsten, diamond, tausonite, cubic zirconia and rutile.

It is worth noting that all GB structures found in the calculation have a considerable excess atomic volume. Large excess volume is usually considered proportional to the degree of segregation (Aaron, Bolling, 1972; Frolov, Mishin, 2012a, 2012b). In case of MgO, this tendency can be implicitly confirmed by experimental studies of grain boundary segregation (Yan et al., 1998b; Wang et al., 2011), where the cavities inside the GB plane act as sinks for point defects. Figure 4 shows the distribution of excess volume υ_{ex}. For each structure, we calculated the GB excess volume as $\upsilon_{ex} = 1/A\left(\mathcal{V} - \mathcal{N} v_{\text{MgO}}\right)$, where $\mathcal{V}$ is the volume of arbitrary chosen region of the structure containing GB plane, $\mathcal{N}$ is the number of atoms in this volume, and v_{MgO} is the volume per atom in bulk MgO. Defined in this way, υ_{ex} represents the deviation of atomic volume in GB region from the bulk. Phase diagram constructed in (υ_{ex}, γ) space allows to study the structural transitions resulting from application of stress σ_{33} in the direction normal to the GB plane. Construction of the convex hull in such a diagram gives information about stable phases at each value of σ_{33}, the stress at which a transition occurs is equal to the negative slope of the corresponding section of the convex hull: $\sigma_{33} = -\partial \gamma / \partial \upsilon_{ex}$.

The values of $\sigma_{33} > 0$ correspond to compression and result in stabilization of dense ID 1421 structure. Negative sign of σ_{33} corresponds to tensile stress. The application of increasingly negative stresses induces complexion transitions, where structures with increasing excess volume are stabilized (ID 402, ID 1270) and finally, the system fractures (ID 605). In other words, analysis of stable GB phases in (υ_{ex}, γ) space may reveal the fracture mechanics at the atomic scale and provide the thermodynamic description of related structural transitions. In particular, one can estimate the value of tensile strength by calculating the slope of the convex
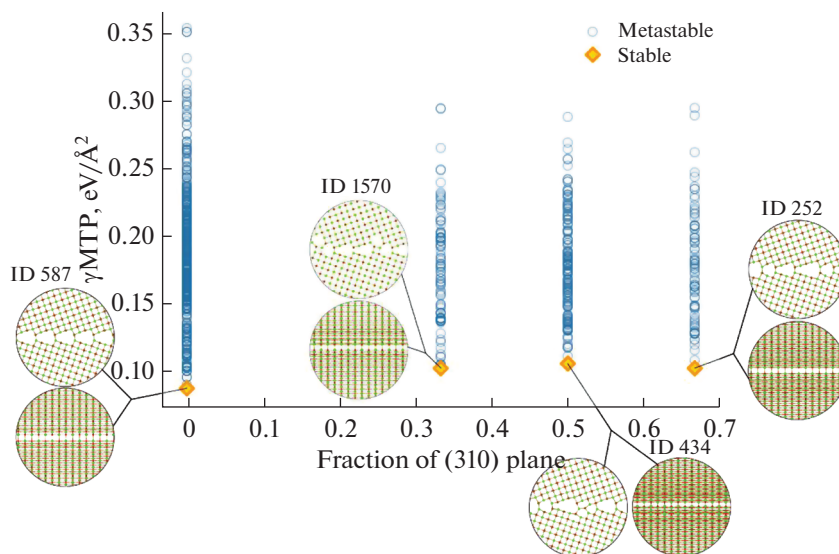
Fig. 2. Phase diagram of the $\Sigma 5(310)[001]$ grain boundary structures in MgO. For each atomic density, the lowest-energy structure is shown by orange diamond. Front and side views of corresponding atomic configurations are given in insets, where magnesium atoms are shown by green spheres and oxygen atoms are shown by small red spheres. IDs of each presented structure are the IDs from evolutionary search. Ground state with $n = 0$ is a CSL-type structure (ID 587). Other newly found structures (ID 1570, ID 434, ID 252) are modifications of the ground state with different atomic densities. They have relatively low interface energies, fairly close to the ground state, which may indicate possible complexion coexistence inside the GB plane.

Рис. 2. Фазовая диаграмма межзеренной границы $\Sigma 5(310)[001]$ в MgO. Для каждой атомной плотности структура с наименьшей энергией показана оранжевым ромбом. Сами структуры показаны во вставках к диаграмме (виды спереди и сбоку), где атомы магния изображены зелеными сферами, а атомы кислорода — красными. Приведенные номера структур (ID) соответствуют их номерам в расчете эволюционным алгоритмом. Основное состояние с $n = 0$ соответствует структуре типа РПС (ID 587). Другие найденные структуры (ID 1570, ID 434, ID 252) являются модификациями основного состояния с различными значениями атомной плотности на границе. Они имеют относительно низкую энергию образования, достаточно близкую к энергии основного состояния, что может свидетельствовать о возможных фазовых превращениях в плоскости границы.

hull section preceding the formation of a crack. The resulting value of $\Sigma 5(310)[001]$ grain boundary tensile strength is 1.14 GPa. Experimental observations (albeit for a different grain boundary) of fracture strength in MgO bicrystals (Ku, Johnston, 1964) range from 0.05 to 0.3 GPa, depending on temperature (T = 300–1400 K) and grain size (D = 1–6 mm). The agreement is good, especially given that tensile strength should significantly decrease with temperature, and should differ for different GBs in the same material.

To sum up, here we demonstrate the application of our newly extended method to the prediction of the atomic structure of grain boundaries and interfaces. Utilizing the natural principles of Darwinian evolution, it is capable of automatically exploring grain boundary configuration space, using only the knowledge of the structure, composition, and orientation of adjacent crystallites. The application of machine learning interatomic potentials makes the study of interfacial structure possible for an arbitrary system of interest almost at *ab initio* level of accuracy. We tested our algorithm on grain boundary complexions in MgO for $\Sigma 5(310)[001]$ orientation. To perform structure relaxation during the evolutionary search, two machine learning interatomic potentials were trained for two successive relaxation stages. The first one was trained on relaxation trajectories of randomly generated MgO crystal structures, and the
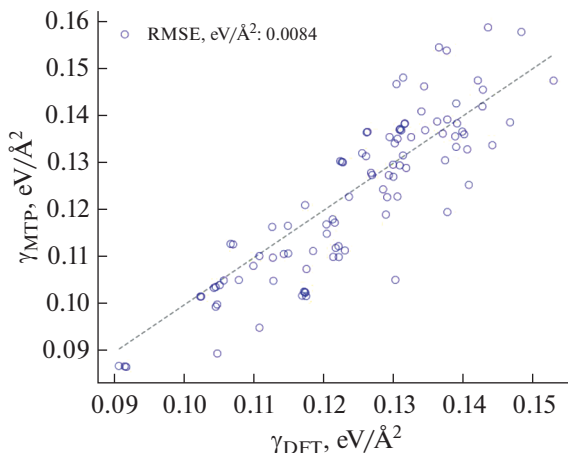
Fig. 3. Comparison of the interface energies predicted with MTP (γ_{MTP}) and calculated with VASP (γ_{DFT}). Each structure is shown as a blue circle, while a dashed gray line shows an ideal target prediction. The root-mean-squared error (RMSE) on MTP predictions is $8.4 \text{ meV}\big/\mathring{A}^2$, or approximately 6.7%.

Рис. 3. Сравнение энергий межзеренных границ, предсказанных с помощью межатомного потенциала MTP (γ_{MTP}) и вычисленных с помощью VASP (γ_{DFT}). Каждая структура показана синим кружком, а серой пунктирной линией отмечено идеальное целевое предсказание. Среднеквадратичная ошибка (RMSE) в предсказании энергии образования составила $8.4 \text{ мэВ}\big/\mathring{A}^2$, или 6.7%.

second one − on molecular dynamics trajectories of MgO supercells with the addition of point defects and random deformations of the cell. Our results confirm that the well known CSL-type structure of $\Sigma5(310)[001]$ GB is the ground state for this orientation, at least in zero-temperature case. In addition to the ground state, several GB complexions with various atomic densities on the boundary plane were found. Moreover, the analysis of grain boundary excess volume revealed the atomistic mechanism of fracture under applied stress. The proposed methodology allows one to thoroughly investigate structures of any crystalline interfaces, which may significantly deepen our knowledge and understanding of this type of systems.

Table 2. Comparison of the values of tilt grain boundary formation energies (γ) in various metals and minerals, calculated using density functional theory (DFT), embedded atom model (EAM) and machine learning interatomic potential (MTP)

Таблица 2. Сравнение энергий образования (γ) наклонных межзеренных границ в различных металлах и минералах, вычисленных с помощью теории функционала плотности (DFT), модели погруженного атома (EAM) и межатомного потенциала на основе машинного обучения (MTP)

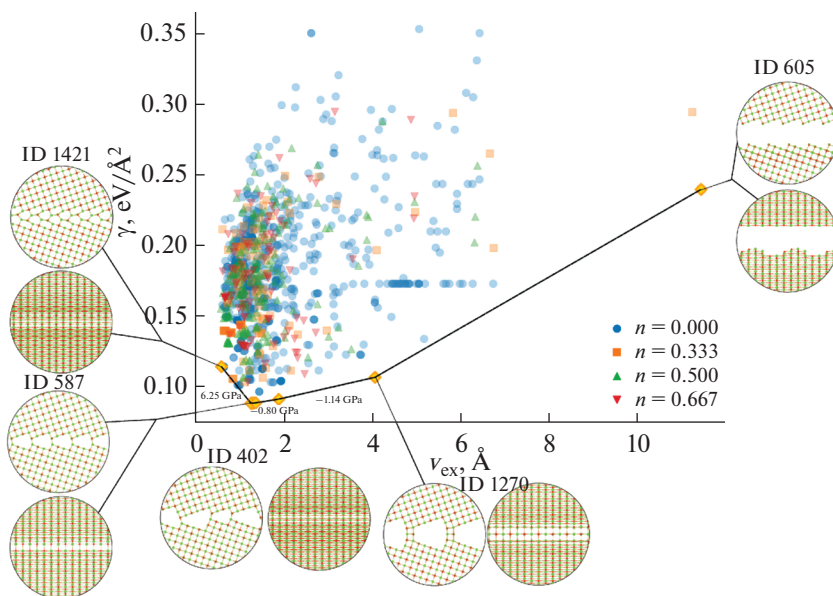| Material	GB	γ, $\text{meV}\big/\mathring{A}^2$	Model	Ref.
Copper (Cu)	$\Sigma5(310)[001]$	56	EAM	(Frolov et al., 2013)
Tungsten (W)	$\Sigma27(552)[1\bar{1}0]$	162	DFT	(Frolov, Setyawan et al., 2018)
Diamond (C)	$\Sigma5(130)[011]$	172	DFT	(Aaron, Bolling, 1972)
Tausonite (SrTiO$_3$)	$\Sigma3(112)[1\bar{1}0]$	72	DFT	(Frolov, Mishin, 2012a, 2012b)
Cubic zirconia (ZrO$_2$)	$\Sigma5(310)[001]$	45	DFT	(Wang et al., 2011)
Rutile (TiO$_2$)	$\Sigma13(221)[1\bar{1}0]$	47	DFT	(Ku, Johnston, 1964)
Periclase (MgO)	$\Sigma5(310)[001]$	86	MTP + DFT	This work

Fig. 4. Phase diagram of the $\Sigma5(310)[001]$ grain boundary in coordinates excess volume (υ_{ex}) − interface energy (γ). Structures with different values of GB atomic density n are represented with colored markers. Convex hull construction (black line) highlights the structures stabilized under stress applied in the direction normal to the GB plane (σ_{33}), which is numerically equal to the negative slope of the convex hull sections. Corresponding values of σ_{33} are given as label of convex hull sections (in GPa): positive sign for compression and negative sign for tension. Applied stress leads to stabilization of dense ID 1421 structure at positive values of stress, or to gradual failure of GB structure (ID 605) with stabilization of intermediate configurations (ID 402, ID 1270) at $\sigma_{33} < 0$. The estimated value of the tensile strength is 1.14 GPa.

Рис. 4. Фазовая диаграмма $\Sigma5(310)[001]$ межзеренной границы в координатах избыточный объем (υ_{ex}) − энергия образования (γ). Структуры с различными значениями атомной плотности на границе n отмечены различным цветом. Выпуклая оболочка на диаграмме (сплошная черная линия) демонстрирует структуры, стабилизирующиеся под воздействием напряжения, направленного вдоль нормали к плоскости границы (σ_{33}), которое численно равно наклону секции выпуклой оболочки со знаком минус. Значение напряжения, соответствующее каждой секции, дано в подписях к графику выпуклой оболочки в единицах ГПа, где положительный знак величины отвечает сжатию структуры, а отрицательный − растяжению. Положительное напряжение приводит к стабилизации структуры ID 1421 отрицательное − к постепенному разрушению границы (ID 605) с несколькими промежуточными структурными превращениями (ID 402, ID 1270) при $\sigma_{33} < 0$. Предел прочности на растяжение составляет 1.14 ГПа.

REFERENCES

Aaron H.B., Bolling G.F. Free volume as a criterion for grain boundary models. *Surf. Sci.* **1972**. Vol. 31. N C. P. 27−49.

Beck P.A., Sperry P.R. Strain induced grain boundary migration in high purity aluminum. *J. Appl. Phys.* **1950**. Vol. 21. N 2. P. 150−152.

Béré A., Chen, J., Ruterana P., Nouet G., Serra A. A step associated with the $\Sigma = 19$ (2530) tilt boundary in GaN. *J. Phys. Condens. Matter.* **2002**. Vol. 14. N 48. P. 12703−12708.

Bollmann W. On the geometry of grain and phase boundaries. *Philos. Mag.* **1967**. Vol. 16. N 140. P. 383−399.

Blöchl P.E. Projector augmented-wave method. *Physical review B.* 1994. Vol. 50(24), P. 17953.

Burke J.E., Turnbull D. Recrystallization and grain growth. *Prog. Met. Phys.* **1952**. Vol. 3. N C.

Bushlanov P.V., Blatov V.A., Oganov A.R. Topology-based crystal structure generator. *Comput. Phys. Commun.* **2019**. Vol. 236. P. 1−7.

Cantwell P.R., Frolov T., Rupert T.J., Krause A.R., Marvel C.J., Rohrer G.S., Rickman J.M., Harmer M.P. Grain boundary complexion transitions. *Annu. Rev. Mater. Res.* **2020**. Vol. 50. P. 465−492.

Cantwell P.R., Ma S., Bojarski S.A., Rohrer G.S., Harmer M.P. Expanding time−temperature-transformation (TTT) diagrams to interfaces: A new approach for grain boundary engineering. *Acta Mater.* **2016**. Vol. 106. P. 78−86.

Cantwell P.R., Tang M., Dillon S.J., Luo J., Rohrer G.S., Harmer M.P. Grain boundary complexions. *Acta Mater.* **2014**. Vol. 62. N 1. P. 1−48.

Chen K.C., Wu W.W., Liao C.N., Chen L., Tu K.N. Observation of atomic diffusion at twin-modified grain boundaries in copper. *Science.* **2008**. Vol. 321. N 5892. P. 1066−1069.

Chen Y., Schuh C.A. Coble creep in heterogeneous materials: The role of grain boundary engineering. *Phys. Rev. B − Condens. Matter Mater. Phys.* **2007**. Vol. 76. N 6. P. 1−13.

Clarke D.R. Varistor Ceramics. *J. Amer. Ceramic Soc.* **1999**. Vol. 82. P. 485−502.

Dey A. Semiconductor metal oxide gas sensors: A review. *Mater. Sci. Eng. B Solid-State Mater. Adv. Technol.* **2018**. Vol. 229. P. 206−217.

Dillon S.J., Harmer M.P. Multiple grain boundary transitions in ceramics: A case study of alumina. *Acta Mater.* **2007**. Vol. 55. N 15. P. 5247−5254.

Dillon S.J., Tang M., Carter W.C., Harmer M.P. Complexion: A new concept for kinetic engineering in materials science. *Acta Mater.* **2007**. Vol. 55. N 18. P. 6208−6218.

Duffy D.M. Grain boundaries in ionic crystals. *J. Phys. C Solid State Phys.* **1986**. Vol. 19. N 23. P. 4393−4412.

Frolov T., Asta M., Mishin Y. Segregation-induced phase transformations in grain boundaries. *Phys. Rev. B − Condens. Matter Mater. Phys.* **2015**. Vol. 92. N 2. P. 1−5.

Frolov T., Asta M., Mishin Y. Phase transformations at interfaces: Observations from atomistic modeling. *Curr. Opin. Solid State Mater. Sci.* **2016**.

Frolov T., Mishin Y. Thermodynamics of coherent interfaces under mechanical stresses. I. Theory. *Phys. Rev. B − Condens. Matter Mater. Phys.* **2012a**. Vol. 85. N 22. P. 224106.

Frolov T., Mishin Y. Thermodynamics of coherent interfaces under mechanical stresses. II. Application to atomistic simulation of grain boundaries. *Phys. Rev. B - Condens. Matter Mater. Phys.* **2012b**. Vol. 85. N 22. P. 224107.

Frolov T., Olmsted D.L., Asta M., Mishin Y. Structural phase transformations in metallic grain boundaries. *Nat. Commun.* **2013**. Vol. 4. P. 1897−1899.

Frolov T., Setyawan W., Kurtz R.J., Marian J., Oganov A.R., Rudd R.E., Zhu Q. Grain boundary phases in bcc metals. *Nanoscale.* **2018**. Vol. 10. N 17. P. 8253−8268.

Frolov T., Zhu Q., Oppelstrup T., Marian J., Rudd R.E. Structures and transitions in bcc tungsten grain boundaries and their role in the absorption of point defects. *Acta Mater.* **2018**. Vol. 159. P. 123−134.

Fujii S., Yokoi T., Yoshiya M. Atomistic mechanisms of thermal transport across symmetric tilt grain boundaries in MgO. *Acta Mater.* **2019**. Vol. 171. P. 154−162.

Harding J.H. Short-circuit diffusion in ceramics. *Interface Science.* **2003**. Vol. 11. P. 81−90.

Harris D.J., Watson G.W., Parker S.C. Atomistic simulation studies on the effect of pressure on diffusion at the MgO 410/[001] tilt grain boundary. *Phys. Rev. B − Condens. Matter Mater. Phys.* **2001**. Vol. 64. N 13. P. 134101.

Hilgenkamp H., Mannhart J. Grain boundaries in high-Tc superconductors. *Rev. Mod. Phys.* **2002**. Vol. 74. N April. P. 485−549.

Kosacki I., Rouleau C.M., Becher P.F., Bentley J., Lowndes D.H. Nanoscale effects on the ionic conductivity in highly textured YSZ thin films. *Solid State Ionics.* **2005**. Vol. 176. N 13−14. P. 1319−1326.

Kresse G., Furthmuller J. Efficient iterative schemes for Ab initio total-energy calculations using a plane-wave basis set. *Phys. Rev. B.* **1996**. Vol. 54. . P. 11169.

Kresse G., Joubert D. From ultrasoft pseudopotentials to the projector augmented-wave method. *Phys. Rev. B.* **1999**. Vol. 59. P. 1758.

Kruglov I.A., Yanilkin A.V., Propad Y., Oganov A.R. Crystal structure prediction at finite temperatures. **2021**. http://arxiv.org/abs/2101.10153

Ku R.C., Johnston T.L. Fracture strength of MgO bicrystals. *Philos. Mag.* **1964**. Vol. 9. N 98. P. 231−247.

Kukli K., Ritala M., Sundqvist J., Aarik J., Lu J., Sajavaara T., Leskelä M., Hårsta A. Properties of hafnium oxide films grown by atomic layer deposition from hafnium tetraiodide and oxygen. *J. Appl. Phys.* **2002**. Vol. 92. N 10. P. 5698−5703.

Langdon T.G. Grain boundary sliding as a deformation mechanism during creep. *Philos. Mag.* **1970**. Vol. 22. N 178. P. 689−700.

Lehockey E.M., Palumbo G., Lin P., Brennenstuhl A. M. On the relationship between grain boundary character distribution and intergranular corrosion. *Scr. Mater.* **1997**. Vol. 36. N 10. P. 1211−1218.

Lejček P., Šob M., Paidar V. Interfacial segregation and grain boundary embrittlement: An overview and critical assessment of experimental data and calculated results. *Prog. Mater. Sci.* **2017**. Vol. 87. P. 83−139.

Lepeshkin S.V., Baturin V.S., Uspenskii Y.A., Oganov A.R. Method for simultaneous prediction of atomic structure and stability of nanoclusters in a wide area of compositions. *J. Phys. Chem. Lett.* **2018**. Vol. 10. N 1. P. 102−106.

Lin P., Palumbo G., Erb U., Aust K.T. Influence of grain boundary character distribution on sensitization and intergranular corrosion of alloy 600. *Scr. Metall. Mater.* **1995**. Vol. 33. N 9. P. 1387−1392.

Lyakhov A.O., Oganov A.R., Stokes H.T., Zhu Q. New developments in evolutionary structure prediction algorithm USPEX. *Comp. Phys. Comm.* **2013**. Vol. 184. N 4. P. 1172−1182.

Maier J. Point-defect thermodynamics and size effects. *Solid State Ionics*. **2000**. Vol. 131. N 1. P. 13−22.

Mazitov A.B., Oganov A.R. Evolutionary algorithm for prediction of the atomic structure of two-dimensional materials on substrates. **2021**. *Cvd*. https://arxiv.org/abs/2103.07677

Meiners T., Frolov T., Rudd R.E., Dehm G., Liebscher C.H. Observations of grain-boundary phase transformations in an elemental metal. *Nature*. **2020**. Vol. 579. N 7799. P. 375−378.

Mott N.F. Slip at grain boundaries and grain growth in metals. *Proc. Phys. Soc.* **1948**. Vol. 60. N 4. P. 391−394.

Musinski W.D., McDowell D.L. Simulating the effect of grain boundaries on microstructurally small fatigue crack growth from a focused ion beam notch through a three-dimensional array of grains. *Acta Mater.* **2016**. Vol. 112. P. 20−39.

Oganov A.R., Glass C.W. Crystal structure prediction using ab initio evolutionary techniques: Principles and applications. *J. Chem. Phys.* **2006**. Vol. 124. N 24. P. 244704.

Oganov A.R., Lyakhov A.O., Valle M. How evolutionary crystal structure prediction works − and why. *Acc. Chem. Res.* **2011**. Vol. 44. N 3. P. 227−237.

Panchal J.H., Kalidindi S.R., McDowell D.L. Key computational modeling issues in Integrated Computational Materials Engineering. *Comput. Des.* **2013**. Vol. 45. N 1. P. 4−25.

Parker S.C., Harris D.J. Computer simulation of general grain boundaries in rocksalt oxides. *Phys. Rev. B − Condens. Matter Mater. Phys*. **1999**. Vol. 60. N 4. P. 2740−2746.

Perdew J.P., Burke K., Ernzerhof M. Generalized gradient approximation made simple. *Physical review letters*. **1996**. Vol. 77(18). P. 3865.

Plimpton S. Fast parallel algorithms for short-range molecular dynamics. *J. Comput. Phys*. **1995**. Vol. 117. N 1. P. 1−19.

Podryabinkin E.V., Shapeev A.V. Active learning of linearly parametrized interatomic potentials. *Comput. Mater. Sci.* **2017**. Vol. 140. P. 171−180.

Pond R.C., Bollmann W. Symmetry and interfacial structure of bicrystals. *Philos. Trans. R. Soc. London. Ser. A, Math. Phys. Sci.* **1979**. Vol. 292. N 1395. P. 449−472.

Pond R.C., Vlachavas D.S. Bicrystallography. *Proc. R. Soc. London, Ser. A Math. Phys. Sci.* **1983**. Vol. 386. N 1790. P. 95−143.

Raj R., Ashby M.F. On grain boundary sliding and diffusional creep. *Metall. Trans.* **1971**. Vol. 2. N 4. P. 1113−1127.

Sangid M.D. The physics of fatigue crack initiation. *Int. J. Fatigue*. **2013**. Vol. 57. P. 58−72.

Sangid M.D., Ezaz T., Sehitoglu H., Robertson I.M. Energy of slip transmission and nucleation at grain boundaries. *Acta Mater.* **2011**. Vol. 59. N 1. P. 283−296.

Shapeev A.V. Moment tensor potentials: A class of systematically improvable interatomic potentials. **2016**. Vol. 14. N 3. P. 1153−1173.

Shimada M., Kokawa H., Wang Z.J., Sato Y.S., Karibe I. Optimization of grain boundary character distribution for intergranular corrosion resistant 304 stainless steel by twin-induced grain boundary engineering. *Acta Mater.* **2002**. Vol. 50. N 9. P. 2331−2341.

Shubnikov A.V., Koptsik V.A. Symmetry in science and art. Moscow: Nauka, 1972 (*in Russian*).

Smith D.A., Pond R.C. Bollmann's 0-lattice theory; a geometrical approach to interface structure. *Int. Met. Rev.* **1976**. Vol. 21. N 1. P. 61−74.

Sutton A.P., Balluffi R.W. Interfaces in Crystalline Materials. Oxford University Press, **1995**.

Suzuki T., Kosacki I., Anderson H.U., Colomban P. Electrical conductivity and lattice defects in nanocrystalline cerium oxide thin films. *J. Am. Ceram. Soc.* **2001**. Vol. 84. N 9. P. 2007−2014.

Tanaka K., Akiniwa Y., Nakai Y., We R.P. Modelling of small fatigue crack growth interacting with grain boundary. *Eng. Fract. Mech.* **1986**. Vol. 24. N 6. P. 803−819.

Uberuaga B.P., Bai X.M. Defects in rutile and anatase polymorphs of TiO_2: Kinetics and thermodynamics near grain boundaries. *J. Phys. Condens. Matter.* **2011**. Vol. 23. N 43.

Uberuaga B.P., Bai X.M., Dholabhai P.P., Moore N., Duffy D.M. Point defect-grain boundary interactions in MgO: An atomistic study. *J. Phys. Condens. Matter*. **2013**. Vol. 25. N 35.

Wang Z., Saito M., McKenna K.P., Gu L., Tsukimoto S., Shluger A.L., Ikuhara Y. Atom-resolved imaging of ordered defect superstructures at individual grain boundaries. *Nature*. **2011**. Vol. 479. N 7373. P. 380−383.

Watanabe T. Grain boundary sliding and stress concentration during creep. *Metall. Trans. A, Phys. Metall. Mater. Sci.* **1982**. Vol. 14 A. N 4. P. 531−545.

Watanabe T., Tsurekawa S. Control of brittleness and development of desirable mechanical properties in polycrystalline systems by grain boundary engineering. *Acta Mater.* **1999**. Vol. 47. N 15. P. 4171−4185.

Watanabe T., Tsurekawa S. Toughening of brittle materials by grain boundary engineering. *Mater. Sci. Eng. A.* **2004**. Vol. 387−389. N 1−2 SPEC. ISS. P. 447−455.

Wynblatt P., Rohrer G.S., Papillon F. Grain boundary segregation in oxide ceramics. *J. Eur. Ceram. Soc.* **2003**. Vol. 23. N 15. P. 2841−2848.

Yan Y., Chisholm M.F., Duscher G., Maiti A., Pennycook S.J., Pantelides S.T. Impurity-induced structural transformation of a mgo grain boundary. *Phys. Rev. Lett.* **1998a**. Vol. 81. N 17. P. 3675−3678.

Yan Y., Chisholm M.F., Duscher G., Pennycook S.J. Atomic structure of a Ca-doped [001] tilt grain boundary in MgO. *J. Electron Microsc.* (*Tokyo*). **1998b**. Vol. 47. N 2. P. 115−120.

Yanev V., Rommel M., Lemberger M., Petersen S., Amon B., Erlbacher T., Bauer A.J., Ryssel H., Paskaleva A., Weinreich W., Fachmann C., Heitmann J., Schroeder U. Tunneling atomic-force microscopy as a highly sensitive mapping tool for the characterization of film morphology in thin high-k dielectrics. *Appl. Phys. Lett.* **2008**. Vol. 92. N 25.

Zhou X.-F., Oganov A.R., Wang Z., Popov I.A., Boldyrev A.I., Wang H.-T. Two-dimensional magnetic boron. *Phys. Rev. B.* **2016**. Vol. 93. N 8. P. 85406.

Zhu Q., Li L., Oganov A.R., Allen P.B. Evolutionary method for predicting surface reconstructions with variable stoichiometry. *Phys. Rev. B.* **2013**. Vol. 87. N 19. P. 195317.

Zhu Q., Samanta A., Li B., Rudd R. E., Frolov T. Predicting phase behavior of grain boundaries with evolutionary search and machine learning. *Nat. Commun.* **2018**. Vol. 9. N 1. P. 1−9.

МЕЖЗЕРЕННЫЕ ГРАНИЦЫ В МИНЕРАЛАХ: АТОМНАЯ СТРУКТУРА, ФАЗОВЫЕ ПЕРЕХОДЫ И ВЛИЯНИЕ НА ПРОЧНОСТЬ ПОЛИКРИСТАЛЛОВ

А. Б. Мазитов[a, b, *], А. Р. Оганов[c, **]

[a]*Московский физико-технический институт, Институтский пер., 9, Долгопрудный, 141700 Россия*

[b]*Всероссийский научно-исследовательский институт автоматики им. Н. Л. Духова (ВНИИА), ул. Сущевская, 22, Москва, 127055 Россия*

[c]*Сколковский институт науки и технологий, Инновационный центр Сколково, ул. Нобеля, 3, Москва, 121205 Россия*

*e-mail: arslan.mazitov@phystech.edu

**e-mail: a.r.oganov@mail.ru

Межзеренные границы (МЗГ) и интерфейсы в поликристаллических материалах являются важными объектами исследований в области материаловедения. Несмотря на более чем 50-летнюю историю их изучения, в данной области остается еще много открытых вопросов. Основной проблемой при изучении структур межзеренных границ является чрезвычайная сложность их экспериментального и теоретического наблюдения и описания. Наличие фазоподобных состояний на границах зерен, называемых комплексиями, лишь усугубляет процесс из изучения. В данной работе мы демонстрируем влияние границ зерен на свойства поликристаллических минералов на примере $\Sigma 5(310)[001]$ границы в периклазе (MgO). Используя комбинацию специально адаптированного под эти цели эволюционного алгоритма USPEX и современных межатомных потенциалов на основе машинного обучения, исследуется конфигурационное пространство указанной межзеренной границы и прогнозируются ее возможные фазовые состояния. В дополнение к широко изученной структуре в модели решетки совпадающих узлов было обнаружено несколько стабильных фаз МЗГ с различными атомными плотностями на плоскости границы. Анализ избыточного объема предсказанных структур границ зерен выявил последовательные стадии разрушения МЗГ при растяжении, приложенном в нормальном направлении к плоскости границы. Наши результаты демонстрируют, что химическое поведение границ зерен и их структурное разнообразие могут быть удивительно богатыми даже в, казалось бы, простых и тщательно исследованных материалах. Явления, которые мы наблюдаем здесь, не являются специфическими для MgO и должны иметь общий характер.

Ключевые слова: предсказание кристаллической структуры, межзеренные границы, комплексии межзеренных границ, машинное обучение, потенциал межатомного взаимодействия, теория функционала плотности